Electrochimica Acta 348 (2020) 136330

Contents lists available at ScienceDirect

Electrochimica Acta

journal homepage: www.elsevier.com/locate/electacta

Quantifying the factors limiting performance and rates in microbial fuel cells using the electrode potential slope analysis combined with electrical impedance spectroscopy

Ruggero Rossi [a], Derek M. Hall [b], Xu Wang [a, c], John M. Regan [a], Bruce E. Logan [a, *]

[a] Department of Civil and Environmental Engineering, The Pennsylvania State University, 231Q Sackett Building, University Park, PA, 16802, USA
[b] EMS Energy Institute, College of Earth and Mineral Sciences, The Pennsylvania State University, 116 Energy and Environment Laboratory, University Park, PA, 16802, USA
[c] School of Resource and Environmental Sciences, Hubei International Scientific and Technological Cooperation Base of Sustainable Resource and Energy, Wuhan University, 129 Luoyu Road, Wuhan, 430079, PR China

ARTICLE INFO

Article history:
Received 10 April 2020
Accepted 26 April 2020
Available online 27 April 2020

Keywords:
Microbial fuel cell
Brush anode
Activated carbon cathode
Charge transfer resistance
Diffusion resistance

ABSTRACT

Improving power generation of microbial fuel cells (MFCs) requires better methods to quantify the impact of the solution chemistry on performance. While buffer concentration and conductivity have been indicated to impact performance of flat (carbon cloth) anodes, we were able for the first to time to quantitatively determine the impact of the phosphate buffer solution (PBS) concentration separate from conductivity on electrode resistances of commonly used brush anodes and activated carbon cathodes. Using the electrode potential slope (EPS) method, we showed that the anode resistance decreased by 64% (from 14.6 ± 0.1 mΩ m^2 to 5.3 ± 0.1 mΩ m^2) by increasing the PBS concentration from 50 to 200 mM. There was no appreciable change in the cathode resistance (17.0 ± 0.1 mΩ m^2, 50 mM; 18.9 ± 0.2 mΩ m^2, 200 mM) although overall performance increased due to a larger cathode experimental working potential ($E_{Cat,e0\text{-}50}$ = 268.9 ± 0.9 mV, $E_{Cat,e0\text{-}200}$ = 370 ± 1 mV). Adding phosphate buffer to low conductivity synthetic wastewater containing 0.25 g L^{-1} sodium acetate decreased the anode resistance by 52% (from 59.1 ± 0.2 mΩ m^2 to 28.1 ± 0.1 mΩ m^2), but increasing only conductivity by adding NaCl or acetate had little impact on electrode resistances. Using electrochemical impedance spectroscopy (EIS), we determined the reasons for these responses. The cathode was limited by oxygen reduction reaction (ORR) kinetics, while the brush anode was limited by mass transfer (proton diffusion), consistent with the impact of buffer concentration on performance. These results have important implications for operation of MFCs as increasing solution conductivity alone, for example, by adding seawater, will not be sufficient to improve anode performance.

1. Introduction

Microbial fuel cells (MFCs) can produce electrical energy from many different substrates including complex organic matter in wastewaters [1]. The biodegradable substrate is oxidized at the anode and the electrons are transferred through an external circuit to the cathode, where the oxygen reduction reaction (ORR) completes the circuit, producing electrical power [2,3]. Improvements in the reactor architecture have resulted in higher power densities, with single-chamber, air-cathode systems producing more power than dual-chamber cells [4]. A standardized laboratory air-cathode MFC architecture has now been extensively used around the world, based on a graphite fiber brush anode and activated carbon (AC) cathode in a small (28 mL) reactor, that has allowed direct comparisons of materials and operational conditions [5]. With this configuration, power densities have exceeded 4 W m^{-2} using a well buffered phosphate solution (PBS), but only reached 0.8 W m^{-2} with typical domestic wastewaters [6,7]. The use of a standardized cell can enable a better understanding of how different solution chemistries can produce these variations in power production, enabling optimization of the system design and operational conditions to improve conversion of the energy in the organic matter into electrical power.

Based on the analysis of electrode resistances, the cathode has

* Corresponding author.
E-mail address: blogan@psu.edu (B.E. Logan).

https://doi.org/10.1016/j.electacta.2020.136330
0013-4686/

often been identified as the main contributor to the cell internal resistance [8,9]. Previous electrochemical impedance spectroscopy (EIS) studies conducted on air cathodes have reported that the major limitation in the cathode performance was the diffusion of oxygen through the diffusion layer [10–14]. However, most of these studies were conducted over a small range of electrode potentials and frequencies. Moreover, the findings were not compared with the results from complementary electrochemical techniques like linear sweep voltammetry (LSV) and polarization data [8]. Understanding the mechanism that limits performance is critical to further improve power production in MFCs. A recently developed method for analyzing MFC performance, called the electrode potential slope (EPS) analysis, can enable quantification of the factors that impact the MFC electrode performance [9]. The method is based on the linearization of the measured electrode potentials, obtained from polarization data, over a current density range near the peak power [9]. The *y*-intercept (zero current) can be used to obtain information about the thermodynamic potential that drives the electrochemical reaction under experimental conditions of interest, while the slope can be used to quantify the area-normalized electrode resistance.

The anode, which can also limit MFC performance, can be impacted by a variety of phenomena due to both biological and chemical operating conditions. For example, anode current production could be limited by an insufficiently developed (thin) biofilm [15], or by inadequate acclimation to operating conditions such as high current densities following prolonged operation at a lower current density [16,17]. Mass-transfer limitations could reduce anode performance, due to limited diffusion of buffer to the electrode [18] with proton accumulation (localized low pH) that could inhibit the anode biofilm current densities, or diffusion of substrate to the biofilm [19,20]. However, most studies that have examined factors that limit anode performance have used different reactor configurations, often with low surface area electrodes such as graphite plates [20], graphite rods [18], or carbon cloth [19]. Using these low surface area anode materials could exaggerate mass-transfer limitations compared to high surface area graphite fiber brushes (areas exceeding 6000 cm^2 per brush) [21]. In other studies it has been indicated that anode performance is kinetically limited [17,22], and thus the relative contributions of diffusion and reaction kinetics remain controversial [23].

In this study, the EPS method and LSV were used in concert with EIS to investigate the behavior of commercial AC cathodes and graphite brush anodes in acetate-PBS and synthetic wastewater-fed MFCs. Using the EPS method enabled quantification of the electrode resistances, while EIS analysis allowed identification of the reaction kinetic and mass-transfer contributions to the electrode resistances determined with the EPS method. This approach provided a comprehensive analysis on the electrode performance limitations in MFCs, which will enable researchers to investigate cell configurations and electrode geometries that reduce the internal losses in small and large scale reactors and improve overall power production.

2. Materials and methods

2.1. Construction and operation of MFCs

MFCs were single-chamber, cubic reactors with a cylindrical internal empty space 4 cm long with a diameter of 3 cm and an empty volume of 28 mL. The anodes were graphite fiber brushes 2.5 cm in diameter and 2.5 cm long, which were made by twisting conductive graphite fibers between two titanium wires [24]. All brushes were heat treated at 450 °C for 30 min in a muffle furnace prior to acclimation [21]. The AC cathodes (7 cm^2 exposed surface area) were manufactured by VITO (Mol, Belgium) with a 70% diffusion layer (DL) porosity. Brush anodes were placed near the cathode (electrode spacing of $d_{An\text{-}Cat} = 1$ cm in phosphate buffer solution (PBS) and $d_{An\text{-}Cat} = 1.3$ cm in synthetic wastewater tests) with the brush perpendicular to the cathode. The larger spacing in synthetic wastewater-fed MFCs was needed to enable initial acclimation of the anodes, as smaller spacing between the electrodes results in larger oxygen contamination of the bioanodes when the solutions have a low chemical oxygen demand (COD) [25]. The ratio between the cathode and the anode projected surface area was 1.4.

Electrochemical tests were conducted using media containing 50 mM PBS (PBS_{50}; 4.58 g L^{-1} Na_2HPO_4, 2.45 g L^{-1} NaH_2PO_4 H_2O, 0.31 g L^{-1} NH_4Cl, 0.13 g L^{-1} KCl, conductivity of 6.93 mS cm^{-1}), 100 mM PBS (PBS_{100}; 9.15 g L^{-1} Na_2HPO_4, 4.90 g L^{-1} NaH_2PO_4 H_2O, 0.62 g L^{-1} NH_4Cl, 0.26 g L^{-1} KCl, conductivity of 11.93 mS cm^{-1}), or 200 mM PBS (PBS_{200}; 18.30 g L^{-1} Na_2HPO_4, 9.81 g L^{-1} NaH_2PO_4 H_2O, 1.24 g L^{-1} NH_4Cl, 0.52 g L^{-1} KCl, conductivity of 20.02 mS cm^{-1}), all at pH = 7.0 ± 0.1. For one test, the 50 mM PBS solution was modified by adjusting the ratio of the phosphate salts to obtain a final pH of 8.0 ± 0.1 ($PBS_{50mM\text{-}pH8}$; 6.62 g L^{-1} Na_2HPO_4, 0.47 g L^{-1} NaH_2PO_4 H_2O, 0.31 g L^{-1} NH_4Cl, 0.13 g L^{-1} KCl, conductivity of 7.97 mS cm^{-1}). For biological tests, these solutions were amended with 12.5 mL L^{-1} of a concentrated trace mineral solution, 5 mL L^{-1} of a vitamin solution, and sodium acetate (1 g L^{-1}) [26].

A synthetic wastewater (SWW) solution was used to maintain a stable composition of the medium over time for the different electrochemical tests. The SWW was prepared based on the average composition of the primary settling effluent of the Pennsylvania State University Wastewater Treatment Plant (Table S1), and it contained: 0.36 g L^{-1} $CaCO_3$, 0.045 g L^{-1} KCl, 0.415 g L^{-1} NaCl, 0.1 g L^{-1} NH_4Cl, 0.011 g L^{-1} K_3PO_4, 0.1 g L^{-1} $MgSO_4$ (conductivity of 1.5 mS cm^{-1}). The solution pH was adjusted to 7.4 with 3 M HCl, and it was amended with 12.5 mL L^{-1} of a concentrated trace mineral solution, 5 mL L^{-1} of a vitamin solution, and sodium acetate (0.25 g L^{-1}). Six MFCs were used for the polarization tests with SWW, and in subsequent tests the same reactors were fed with SWW amended with 50 mM phosphate buffer (SWW/PB; 4.58 g L^{-1} Na_2HPO_4, 2.45 g L^{-1} NaH_2PO_4 H_2O, conductivity of 7.2 mS cm^{-1}) to examine the impact of buffer capacity, NaCl (SWW/NaCl; 1.49 g L^{-1} NaCl, conductivity of 7.2 mS cm^{-1}) to increase conductivity, or sodium acetate (SWW/NaAc; 0.25 g L^{-1} additional NaAc, or 0.50 g L^{-1} total) to examine the impact of substrate concentration on anode performance. One test was conducted using the SWW/PB solution amended with additional 0.25 g L^{-1} sodium acetate (0.50 g L^{-1} sodium acetate total) to determine the effect of both substrate concentration and a well-buffered SWW (Supporting Information). The solution pH and conductivity were monitored using a probe and meter (Seven-Multi, Mettler-Toledo International Inc., USA).

The MFCs were operated in duplicate at 30 °C in a controlled temperature room. Anodes were acclimated as previously described for more than one year while used in other studies [9,27]. Graphite fiber brushes fed for >1 year with acetate in PBS were used for the analysis with PBS, while brushes fed for >1 year with wastewater were used for the analysis in SWW. The reactors were inoculated with effluent from other MFCs and operated in batch mode at 1000 Ω external resistance. Two days before each electrochemical test, the external resistance was decreased to 500 Ω overnight and 100 Ω for the rest of the day to acclimate the biofilm at larger current densities as previously described [28].

2.2. Electrochemical measurements

The tests on the cathodes (in duplicate) were conducted in a cylindrical electrochemical cell 4 cm long with a diameter of 3 cm and an empty volume of 28 mL with the cathode as the working

electrode and a Pt mesh (3 cm^2 projected area) as a counter electrode, placed 3 cm far from the cathode. The reference electrode (RE) used to measure the electrode potentials (Single junction silver chloride (Ag/AgCl) reference electrode; model RREF0021, Pine Research Instrumentation, NC; + 199 mV versus a standard hydrogen electrode, SHE) was placed in the current path between the electrodes, 1 cm distant from the cathode [29]. All potentials are reported here versus SHE. An anion exchange membrane (Selemion AMV, Asahi Glass, Co., Tokyo, Japan) was placed between the cathode/RE chamber and the Pt counter electrode when electrochemical tests were conducted on the cathode. This configuration allowed evaluation of the cathode performance and avoided damaging the biofilm on the brush anode, commonly used as counter electrode, as it was observed in preliminary tests that spectra obtained at low frequencies produced an irreversible drop in anodic current production. The electrochemical analyses on the anode were conducted in an operating, single-chamber MFC with the anode as the working electrode, the cathode as the counter electrode, and the RE tip touching the titanium wire [30].

Cathodic LSVs at a scan rate of 0.1 mV s^{-1} were registered from the open circuit potential (OCP) to −200 mV, while anodic LSVs were obtained from the OCP to −100 mV. Prior to LSVs the working electrodes were left for 2 h at the OCP and then a fast EIS (from 100 kHz to 500 Hz, 5 mV amplitude, 10 points s^{-1}, ≈25 s $scan^{-1}$) was recorded at the OCP to calculate the solution resistance (R_Ω). The reported electrode potentials were corrected based on R_Ω [30]. The measured electrode potentials (not corrected for R_Ω) are reported in the Supporting Information. The current was normalized by the geometric cross-sectional area of the MFC (A = 7 cm^2).

The performance of the electrodes was examined using the EPS method [9,31]. Briefly, following a rapid variation in potential due to activation losses over the initial small increase in current, the system was operated under steady-state conditions. The slopes of the linearized portion of the electrode potentials were used to express the performance of the anode and cathode as two resistances, with the solution resistance and the membrane (if present) as the final component of the total internal resistance of the cell [9,31]. The linearized portion of the electrode potential in polarization plots, as a function of current density, was fitted by $E = m\ j + b$, where j is the current density (A m^{-2}), the absolute value of the slope m is defined as the specific resistance of the anode (R_{An}) or cathode (R_{Cat}) in units of mΩ m^2, and the y-intercepts are used to calculate the experimental open circuit potentials of the anode ($E_{An,e0}$) or cathode ($E_{Cat,e0}$). A schematic representation of the parameters used for the EPS analysis is reported in the Supporting Information. Using the linearized portion of the electrode potential near the maximum power, it is possible to reproduce the power density curve in polarization tests [9].

The typical reactions in an MFC are acetate oxidation at the anode and the ORR at the cathode, which can proceed through different pathways resulting in 4 or 2 electrons transferred per molecule of O_2 consumed:

$$CH_3COO^- + 4H_2O \rightleftharpoons 2H_2CO_3 + 8e^- + 7H^+ \quad E_{An} = -296\ mV \tag{1}$$

$$O_2 + 4e^- + 2H_2O \rightleftharpoons 4OH^- \quad E_{Cat} = +815\ mV \tag{2}$$

$$O_2 + 2e^- + 2H^+ \rightleftharpoons H_2O_2 \quad E_{Cat} = +282\ mV \tag{3}$$

$$O_2 + 2e^- + 2H_2O \rightleftharpoons H_2O_2 + 2OH^- \quad E_{Cat} = +267\ mV \tag{4}$$

$$O_2 + 2e^- + H_2O \rightleftharpoons HO_2^- + OH^- \quad E_{Cat} = +337\ mV \tag{5}$$

where the standard electrode potentials are given versus SHE at pH 7. The LSVs registered in PBS were linearized over a 5–9 A m^{-2} range while tests with SWW were linearized over a 0.7–2.0 A m^{-2} range, as these were the current density ranges where the maximum power densities occurred using these media [9].

EIS measurements were conducted at different applied potentials for the anode and the cathode over a frequency range of 100 kHz to 5 mHz, applying a sinusoidal perturbation of 5 mV amplitude and registering 10 points per decade. Prior to the EIS analysis the working electrode was left for 2 h at OCP and then the electrode potential correspondent to that of the EIS was set for 30 min. The Nyquist plots of the impedance data were analyzed with Zfit provided in the EC-lab software (Bio-Logic USA) and the equivalent circuits reported in the Supporting Information were used to obtain the value of the electrochemical components.

2.3. Calculations

The diffusion layer thickness, d, was estimated as

$$d = \left(D_{lim}\ t_{diff}\right)^{1/2} \tag{6}$$

where D_{lim} is the diffusivity of the limiting chemical species (acetate, 1.10 × 10^{-5} cm^2 s^{-1}; protons, 9.13 × 10^{-5} cm^2 s^{-1}; hydroxyl, 5.16 × 10^{-5} cm^2 s^{-1}) [32], and t_{diff} is the characteristic time of the diffusion calculated from the characteristic frequency of diffusion using the EIS spectra [33–35]. The magnitude of t_{diff} is affected by the frequency at which the diffusion occurs, and therefore it is dependent by the operational parameters and by the diffusing species [36]. An example calculation is shown in the Supporting Information (Fig. S1).

The concentration in the bulk solution of the chemical species diffusing through the diffusion layer c_{lim} was calculated [33,35,37] as:

$$c_{lim} = \frac{RTd}{z^2F^2\ D_{lim}\ R_d\ s} \tag{7}$$

where T is the temperature (K), R is the gas constant (J mol^{-1} K^{-1}), z is the number of electrons transferred (8 for acetate oxidation), F is the Faraday constant (A s mol-e^{-1}) and s is effective surface area of the electrode (cm^2). The effective area of the electrode must be used here rather than the projected area, as the electrochemical reaction rate is dependent on the actual area of the electrode in contact with the electrolyte. A value for s was estimated from the effective capacitance of the double layer obtained by fitting the spectra and assuming a capacitance for a flat carbon electrode of 10 μF cm^{-2} [33,37,38]. The effective capacitance of the cathodes was calculated based on a surface distribution through the Brug equation due to the large porosity of the AC, while the anode effective capacitance was calculated based on a normal distribution due to the low porosity of the graphite bristles and a negligible solution resistance [8,39,40].

3. Results and discussion

3.1. Impact of buffer concentration on the cathodic polarization behavior

The main change that occurred at the cathode as a result of the increase in buffer concentration was the increase in the

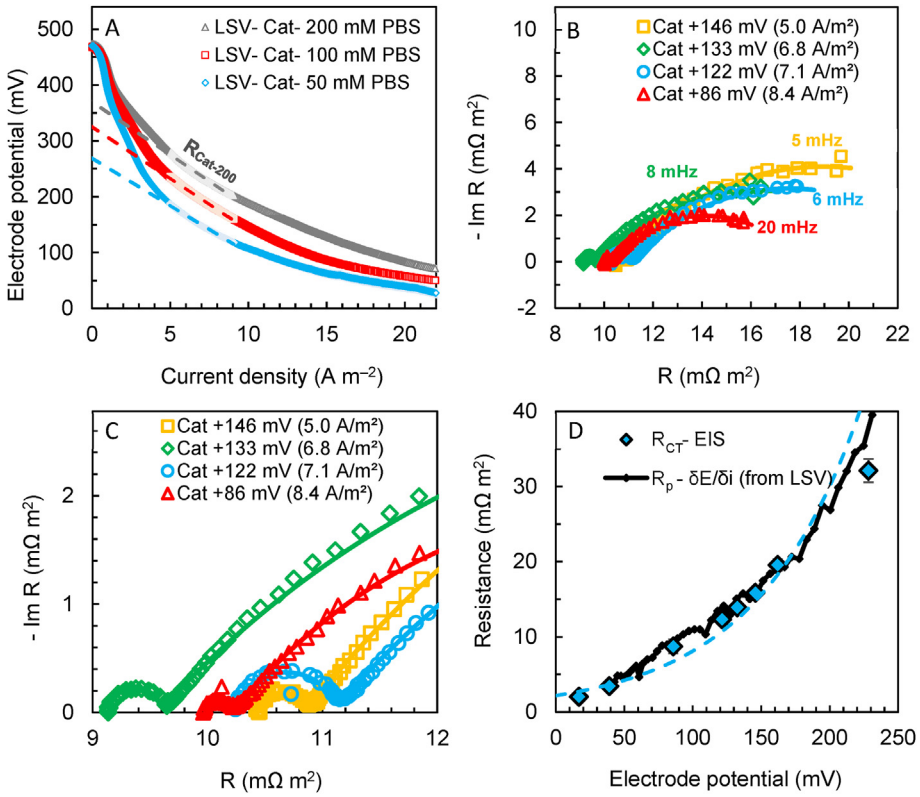

Fig. 1. (A) Cathodic linear sweep voltammetries in PBS at different concentrations (50 mM, 100 mM, and 200 mM) following corrections for the solution resistance. The dashed lines represent the linearization of the data in the 5–9 A m^{-2} region. Cathode potentials not corrected for ohmic losses are reported in the Supporting information (Fig. S2). (B) Cathode EIS spectra in 50 mM PBS. Solid lines represent the fitting to the spectra. The characteristic frequencies given in the plot for each spectrum correspond to the maximum in the imaginary impedance. (C) Enlargement of the cathode EIS spectra at high frequencies. (D) Correspondent cathodic charge transfer (R_{CT}) obtained from the fits of the EIS spectra and the polarization resistance (solid black line- R_p) calculated from the slope of the LSV as $\delta E/\delta i$. The dashed blue line represents the exponential trendline obtained from the R_{CT}. The overpotential can be calculated from OCP = 470 ± 3 mV. (For interpretation of the references to color in this figure legend, the reader is referred to the Web version of this article.)

experimental potentials, measured by the *y*-intercept of the linearized portion of the elecrode potential (Fig. 1A). For example, the cathode potential increased by 21% in 100 mM PBS ($E_{Cat,e0\text{-}100}$ = 325 ± 1 mV) compared to the 50 mM buffer ($E_{Cat,e0\text{-}50}$ = 268.9 ± 0.9 mV), and by 38% in 200 mM PBS ($E_{Cat,e0\text{-}200}$ = 370 ± 1 mV). There was no change in the OCP or the cathode area resistance. The cathodic measured OCPs were essentially constant at ~470 mV ($E_{Cat,m0\text{-}50}$ = 470 ± 3 mV; $E_{Cat,m0\text{-}100}$ = 468 ± 5 mV; $E_{Cat,m0\text{-}200}$ = 474 ± 7 mV) since the concentration of the species involved in the electrochemical reaction (Eqs. (2)–(5)) did not change. There was also no change in the cathodic resistance R_{Cat} with the buffer concentration at high currents, as shown by similar slopes in the cathode polarization data. The cathode resistance in 50 mM PBS buffer ($R_{Cat\text{-}50}$ = 17.0 ± 0.1 mΩ m^2) was only slightly less than that in 100 mM ($R_{Cat\text{-}100}$ = 18.5 ± 0.1 mΩ m^2) or 200 mM ($R_{Cat\text{-}200}$ = 18.9 ± 0.2 mΩ m^2) buffer solutions.

Two different regions have been identified in the LSVs and Tafel plots of the cathode (Fig. 1A, Fig. S5), a low-current density region (<2 A m^{-2}) with small Tafel slopes, and a high current density (between 3 and 20 A m^{-2}) region with larger Tafel slopes. The concentration of the buffer appears to impact the lower Tafel slope values, suggesting that a pH-dependent species is involved [41]. However, the high current density region does not appear to depend on the buffer concentration. Although the rate determining step (RDS) is not known, it is clear that increasing the buffer concentration altered the influence of one or more RDSs on the ORR kinetics, as shown by improved experimental cathode potentials with buffer concentration. This improved ORR moved the kinetics closer to that of a 4 e$^-$ transfer (+815 mV, eq. (2)), compared to the lower potentials when there is a 2 e$^-$ transfer (+282 V, +267 V, and +318 V, eqs. (3)–(5)). A rise in the local pH near the cathode has been shown in other studies using Pt/C cathodes, with increases in pH correlated to a reduction in ORR thermodynamic potential in MFCs. For example, in 100 mM PBS the pH at the cathode increased from 7 to 10 at 4 A m^{-2}, and from 7 to 12 at 10 A m^{-2} [42]. Each increment of pH unit will decrease the cathodic potential by 59 mV at room temperature, based on the Nernst equation. Thus, only the experimental cathode potentials were impacted by the concentration of the buffer solution, and not electrode resistances.

EIS analysis of the cathode provided additional direct evidence that the main source of the cathode resistance at operating potentials of interest was reaction kinetics and not mass transfer limitations (Fig. 1B). EIS spectra were obtained at different cathode potentials in 50 mM PBS (Fig. S3). Complex plane plots showed a first x-axis intercept, followed by two semi-circles, the first at high frequencies with a smaller radius that did not noticeably change at different applied potentials, and a second large and slightly depressed semicircular arc dominating the Nyquist diagrams (Fig. 1B). The first intercept of the spectra with the real impedance axis, which is the solution resistance (R_Ω), changed (range of 9.0 ± 0.5 mΩ m^2 to 10.8 ± 0.8 mΩ m^2) (Fig. 1C) by an amount (<2 Ω) that could be due to small variations in the distance between the RE and working electrodes (e.g., 1 mm in 50 mM PBS, with 6.93 mS cm^{-1}) [30].

The first small semicircle (high frequencies) was consistent with the effect of a porous electrode on the EIS spectra rather than an electrochemical reaction. This semi-circle showed a good fit to a Q_1/

R_1 element in the circuit (Fig. S4), with an effective capacitance ($Q_1 = 0.24 \pm 0.06$ F m^{-2}) and resistance ($R_1 = 0.61 \pm 0.20$ mΩ m^2) that varied very little over the applied potentials. Due to its independence of the set electrode potential, this capacitance and resistance was concluded to be due to the high electrode porosity over the electroactive region [33,43]. The second semicircle (low frequencies) represents the ORR reaction kinetics, decreasing at less positive potentials and larger current densities, indicating the absence of mass transfer limitations as shown by the lack of limiting current densities in the LSVs (Fig. 1B). This electrochemical process was fitted to a Q_{DL}/R_{CT} element, following the ohmic Q_1/R_1 element (Fig. S4). As the applied potential was decreased, the correspondent R_{CT} exponentially diminished with it, a pattern that is consistent with a kinetically-controlled process in the Tafel region in the absence of mass transfer limitations [44]. The reason for the absence of diffusion limitations could be due to the high surface area of the activated carbon, making the catalytic sites more accessible to the reactants, avoiding diffusion limitations in the current density range more common to MFCs [9,43].

As current increases, mass transfer limitations will eventually occur [44]. However, because the second semicircle never intercepted the real impedance axis at low frequencies (i.e. the imaginary part of the impedance was always positive) (Fig. 1B), it is not clear whether the spectra examined here captured all the electrochemical processes, such as a diffusion-controlled process following the kinetic one at low frequencies (<5 mHz). To further investigate if the EIS analysis had captured all relevant processes, we compared R_{CT} with the polarization resistance at each applied potential (R_p), calculated from the slope of the polarization curve ($\delta E/\delta i$). The R_p term includes both reaction kinetic and mass transfer contributions to the overall resistance [34,37,44]. A comparison of R_p with R_{CT} showed good agreement between these values (Fig. 1D), indicating that nearly all the polarization resistance R_p was due to R_{CT} and thus reaction kinetics. The agreement between R_{CT} and R_p shows an absence of a contribution of diffusion limitations at low frequencies to the overall electrode performance, and thus it can be concluded that the cathode resistance R_{Cat} was only due to the kinetic limitations of the ORR at current densities of >3 A m^{-2}. At the very lowest current densities of <1.4 A m^{-2} with 50 mM buffer, in the region where activation losses predominate, a third semicircle arises at very low frequencies (0.1 mHz) (Fig. S5). The emergence of this further semicircle suggests an additional reaction that may arise at low current densities, in agreement with the two slopes obtained from Tafel plots (Fig. S5), where the concentration of the buffer is critical for maintaining circumneutral pH. Due to the long scan times needed for this analysis (>26 h), this low current density region was not further explored.

3.2. Impact of buffer concentration on the anodic polarization behavior

In sharp contrast to the cathode results, the anode peformance was strongly influenced by buffer concentration over all current densities (Fig. 2A). There was no change in the anode OCP, and only

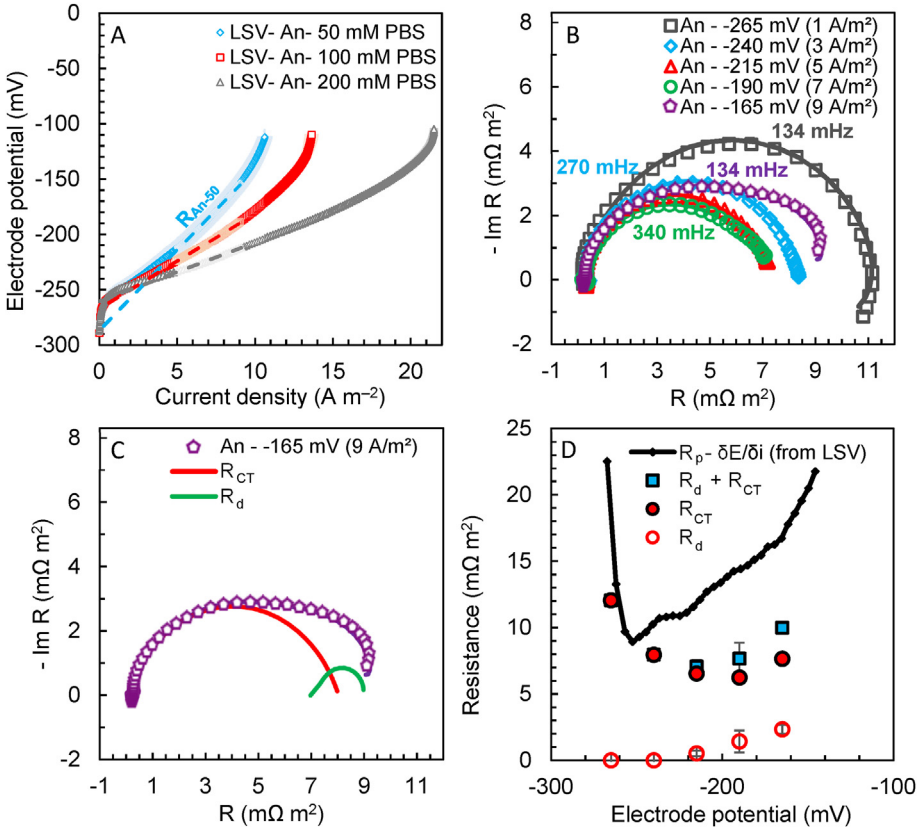

Fig. 2. (A) Anodic linear sweep voltammetries in PBS at different concentrations (50 mM, 100 mM, and 200 mM) following corrections for the solution resistance. The dashed lines represent the linearization of the data in the 5–9 A m^{-2} region. Anode potentials not corrected for ohmic losses are reported in the Supporting information (Fig. S2). (B) Anode EIS spectra in 50 mM PBS. Solid lines represent the fitting to the data. The characteristic time frequencies (numbers in mHz) correspond to the maximum in the imaginary impedance for the different spectra in the graph with the same color. (C) Visual presentation of the charge transfer (R_{CT}) and diffusion (R_d) components of the resistance to the total EIS spectrum at −165 mV (9 A m^{-2}). (D) Anodic R_{CT} and R_d resistances, obtained from the EIS spectra, and polarization resistance (solid black line- R_p) calculated from the slope of the LSVs as $\delta E/\delta i$. The overpotential can be calculated from the OCP = −288 ± 2 mV. (For interpretation of the references to color in this figure legend, the reader is referred to the Web version of this article.)

a small change in the working electrode potential of the 50 mM PBS relative to the other two concentrations, primarily due to the very rapid rise of the potential with current densities. The lack of a change in the potentials reflects the presence of a single oxidation reaction for acetate at the anode (Eq. (1)), compared to mutliple possible reactions on the cathode.

The impact of buffer concentration can be seen by the large changes in the anode area-resistances from EPS analysis. The anode resistance decreased by 41% in 100 mM ($R_{An\text{-}100} = 8.62 \pm 0.08$ mΩ m^2) and an additional 39% in 200 mM buffer ($R_{An\text{-}200} = 5.3 \pm 0.1$ mΩ m^2), compared to that in 50 mM PBS ($R_{An\text{-}50} = 14.6 \pm 0.1$ mΩ m^2). The LSVs also showed limiting current densities, as shown by very little change in current densities at the highest values for more positive potentials, suggesting mass-transfer limitations. These limiting current densities increased with buffer concentration, ranging from 10.6 ± 0.5 A m^{-2} in 50 mM PBS, to 13.7 ± 0.5 A m^{-2} in 100 mM PBS and 21.5 ± 0.3 A m^{-2} in 200 mM PBS.

Although increases in anodic limiting current density have been previously reported for MFCs with high buffer concentrations (≥100 mM PBS) [18,20], the reasons for the these changes remain controversial as both biological and physical explanations have been suggested. For example, high current generation could be limited by bacterial kinetics for different microorganisms [15] or an inadequate acclimation of the biofilm to high current densities [16]. Alternatively, current was suggested to be limited by mass transfer limitations, due to insufficient proton transport resulting in the localized acidification of the biofilm [18–20], but other studies suggested these physical factors were unimportant [17,22]. Unfortunately, the large variability in the MFC architectures used among these studies makes the results difficult to directly compare. For example, the low surface area of the anodes used in some studies, such as graphite rods [18], graphite plates [20], or carbon cloth [19], could exaggerate mass transfer limitations relative to higher surface area electrodes such as brush anodes.

To investigate the importance of reaction kinetics versus mass transfer for the anode in 50 mM PBS, EIS data were obtained at electrode potentials between −265 mV and −165 mV (Fig. 2, Fig. S6). At high frequencies EIS spectra for the anode showed a non-linear behavior (Fig. S7), likely due to the presence in the anode of the twisted Ti wire and the high surface area graphite bristles. It was previously reported that the presence of different materials in the anode, for example carbon felt and Ti wire current collector, contributed to alter the shape of the spectra with each element contributing with its charateristic frequency to the spectra [17]. Modeling this part of the spectrum at higher frequencies is further discussed in the Supporting information (Fig. S8). At lower frequencies and current densities <5 A m^{-2}, complex plane plots showed a single large and slightly depressed arc at each set potential that intercepted the real impedance axis. However, when the applied potential became more positive, at current densities >5 A m^{-2}, a second process appeared at low frequencies (Fig. 2B and C) which is evidenced by a shift of the real part of the impedance towards higher resistances at low frequencies (Fig. 2B and C), at −215 mV (5 A m^{-2}), −190 mV (7 A m^{-2}), and −165 mV (9 A m^{-2}). The large semicircle dominating the spectra was due to the kinetics of the electrochemical acetate oxidation by the bacteria (Q_{DL}/R_{CT}).

At electrode potentials more positive than − 215 mV (5 A m^{-2}) another process followed the reaction kinetics at higher current densities, which was consistent with mass-transfer limitations (Fig. 2C, Fig. S1). To include this additional process of mass transfer resistance, a diffusion element was included in the equivalent circuit in series to the charge transfer resistance, in parallel with the constant phase element ($Q_{DL}/R_{CT} + Z_d$) (Fig. S8) [8]. The magnitude of the correspondent diffusion resistance (R_d) increased as the electrode potential was shifted toward more positive and higher current densities, reaching a maximum at − 165 mV (9 A m^{-2}) (Fig. 2D).

The charge transfer resistance (R_{CT}) accounted for 83% of the sum of $R_d + R_{CT}$ in the current density range 5–9 A m^{-2}, indicating that charge transfer was the main contributor to the anode resistance in 50 mM PBS. However, R_{CT} did not exponentially decrease by applying more positive potentials (Fig. 2D) as it has been observed for the cathode (Fig. 1D), thus the diffusion process was limiting the kinetic process. R_{CT} decreased by 49% by increasing the anode potential from −265 mV to −190 mV (from 12.1 ± 0.3 mΩ m^2 to 6.2 ± 0.4 mΩ m^2) (Fig. 2D). At the most positive potential (−165 mV, 8.97 ± 0.03 A m^{-2}) and highest current density, R_{CT} increased back by 23% to 7.65 ± 0.04 mΩ m^2. The increment in R_{CT} over the range of potentials of −190 mV to −165 mV can be explained by the adverse effects of ion transport (mass transfer) on bacterial kinetics. Mass-transfer limitations (green line in the spectrum in Fig. 2C) were identified by changes in the diffusion resistance R_d in the spectra at anode potentials more positive than −215 mV, where R_d increased by 460% from 0.5 ± 0.2 mΩ m^2 (−215 mV) to 2.3 ± 0.3 mΩ m^2 at −165 mV (Fig. 2D).

Diffusion of protons can be deduced to be the main reason for the mass-transfer limitations of the anode at high current densities. The concentration of the limiting species calculated with eq. (7) at the different potentials ranged between $4.3 \pm 0.3 \times 10^{-7}$ M and $7.0 \pm 0.1 \times 10^{-8}$ M, which corresponds well to the concentration of protons at a pH of ~7. The electrochemically active surface area in eq. (7) was calculated from the electrode capacitance as 5030 ± 1440 cm^2, by assuming a surface capacitance of a flat carbon electrode of 10 μF cm^{-2} [33,37,38]. The large variability in the calculated surface area, as shown by the large standard deviation, was due to an increase in the double layer capacity of the carbon with overpotential due to its space charge as a semiconductor [33,45,46]. This brush surface area is in reasonable agreement with the surface area obtained from BET analysis of heat treated carbon brush anodes (7590 cm^2) [21,24], when considering that only half of the brush has been shown to be involved in the electrochemical reactions [10]. The average diffusion layer thickness was 290 ± 30 μm, and the possibility of OH^- being the limiting specie was excluded by performing EIS at pH 8, which showed a decrease in the concentration of the limiting species from pH 7 to pH 8 (Fig. S9). These results were in good agreement with the large impact of the buffer concentration obtained from LSVs (Fig. 2A), as the buffer would mitigate pH changes. Thus, the mass-transfer limitations at the brush anode were concluded to be due to the accumulation of H^+ near the biofilm.

To examine if the EIS analysis captured all the electrochemical processes relevant to anode performance, we compared R_{CT} and R_d with the total polarization resistance at each applied potential (R_p) calculated from the slope of the polarization curve ($\delta E/\delta i$). Since the sum of R_{CT} and R_d was less than R_p, there likely was an additional process that was not captured by the above EIS analysis in the frequency range investigated here (Fig. 2D, Fig. S8). To try to detemine the nature of that process, we obtained additional EIS spectra at < 5 mHz that showed a consecutive arc that we fitted with an additional element in the circuit (Q_7/R_7) (Fig. S8, Fig. S10). However, this portion of the curve could not be completely examined further due to the very long times needed to obtain these spectra (for example, >26 h at frequencies up to 0.1 mHz) as the anode potentials would not be stable over these periods of time due to depletion of substrate in the solution. Thus, this additional contribution to the anode resistance was not further examined here.

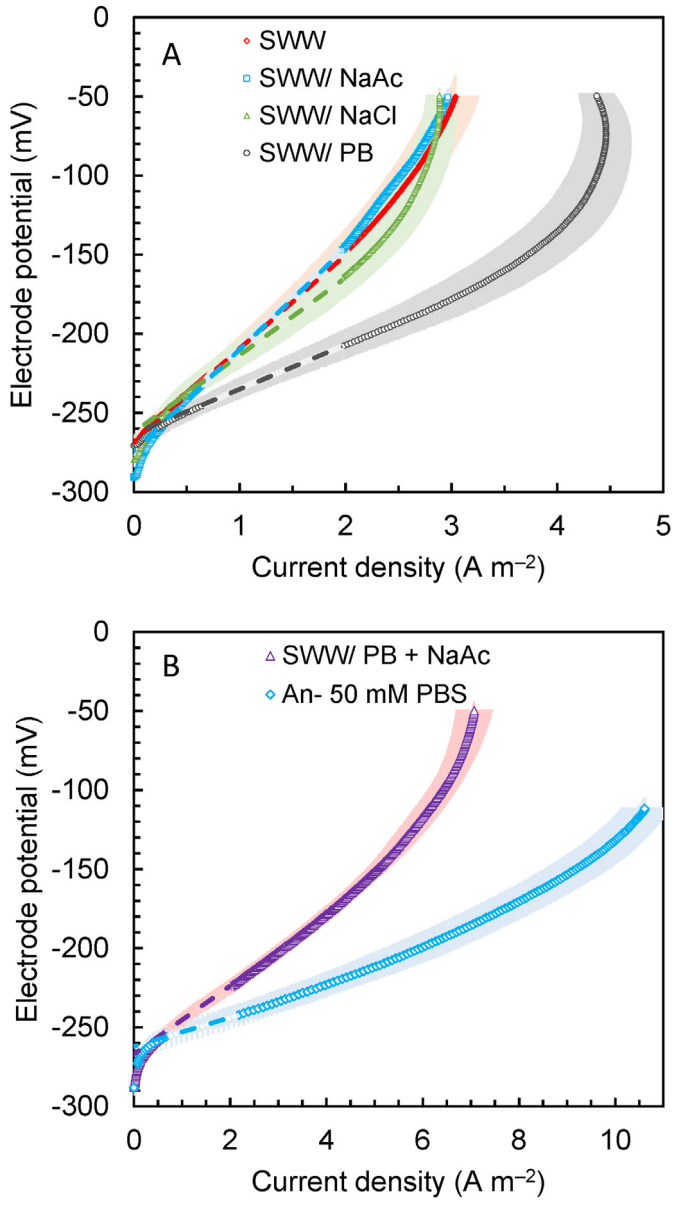

Fig. 3. (A) Anodic linear sweep voltammetries in synthetic wastewater (SWW) or SWW amended with 0.50 g/L of sodium acetate (SWW/NaAc), sodium chloride (SWW/NaCl), or phosphate buffer (SWW/PB), following correction for solution resistance. The dashed lines represent the linearization of the data in the 0.7–2.0 A m^{-2} region. Anodic LSVs not corrected for ohmic losses are reported in the Supporting information (Fig. S12). (B) Anodic LSVs in synthetic wastewater (SWW) amended with PB and with 0.5 g L^{-1} (SWW/PB + NaAc) of acetate in respect to that obtained in 50 mM PBS with anodes fed with PBS for more than one year (Fig. S13). The dashed lines represent the linearization of the data in the 0.7–2.0 A m^{-2} region.

3.3. Anode performance in low conductivity synthetic wastewater

Treatment of domestic wastewaters using MFCs is often hampered by the low conductivity (~1–1.5 mS/cm) and low substrate concentration (COD <0.4 g/L) of the solutions [47]. To identify which factors are most important for MFCs used to treat wastewater, tests were conducted with a SWW solution with representative concentrations of acetate (0.25 g L^{-1}) and buffer (conductivity of 1.5 mS cm^{-1}). Current densities were greatly reduced with SWW compared to that with 1 g L^{-1} acetate in 50 mM PBS (Fig. 3). For example, the anode resistance increased to 59.1 ± 0.2 mΩ m^2 in SWW compared to only 9.08 ± 0.08 mΩ m^2 for 50 mM PBS and 1 g L^{-1} of acetate in the same current density range (0.7–2 A m^{-2}) (Fig. 3). This anode resistance using SWW was slightly lower than that previously reported using actual domestic wastewater (75 ± 9 mΩ m^2) [9].

Amending the SWW with PBS to increase its buffering capacity decreased the anode resistance by 53% to R_{An} = 28.1 ± 0.1 mΩ m^2 (SWW/PB). However, increasing the solution conductivity using NaCl to match that of the SWW/PB, or increasing the acetate concentration to 0.50 g L^{-1} had a minimal impact on the performance ($R_{An\ SWW\text{-}NaCl}$ = 48.9 ± 0.2 mΩ m^{-2}, $R_{An\ SWW\text{-}NaAc}$ = 64.1 ± 0.1 mΩ m^2, SWW/NaAc). The limiting current density of the amended SWW/PB was similarly much improved (4.4 ± 0.2 A m^{-2}) compared to those without the buffer and with extra acetate (3.0 ± 0.1 A m^{-2}) or NaCl (2.9 ± 0.1 A m^{-2}) (Fig. 3).

These results demonstrate that anodic performance was limited primarily by the low buffer capacity of the wastewater (which for an actual wastewater would be its alkalinity) [48] and not conductivity. This finding is contrary to previous claims that performance using wastewater compared to 50 mM PBS solutions was solely due to the reduced substrate concentration or solution conductivities [49,50]. Here, the concentration of the substrate did not impact current densities obtained with acetate concentrations of 0.25 g L^{-1} or 0.5 g L^{-1}, and additional NaCl did not appreciably impact performance.

3.4. Overall assessment of factors impacting MFC performance

The analysis of the electrodes using both the EPS and EIS methods provided definite evidence that the anode and cathode are limited by two different mechanisms. The cathode performance was completely controlled by ORR kinetics, rather than mass transfer, as shown by insensitivity of the electrode resistance (slope in the EPS analysis) to buffer concentration and nearly all of the polarization resistance could be accounted for by just the charge transfer resistance in the EIS analysis. This finding is different than the conclusion reached by others that performance of AC cathodes in MFCs are limited by diffusion of oxygen or hydroxyl ions [10–14,42]. As current densities increased and the localized pH around the cathode increased, the cathodic reaction shifted between two different rate determining steps, as evidenced by changes in the slopes in Tafel plots.

The performance of the anode, in contrast to that of the cathode, was primarily limited by diffusion of protons from the electrode, despite the high anode surface area. The anode resistances showed a clear and favorable response to increased concentrations of buffer in the EPS analysis. There is only a single anode reaction pathway for acetate oxidation, versus multiple reaction pathways possible at the cathode for the ORR. Thus, the anode performance was closely associated with the concentration of a strong buffer. EIS analysis showed that charge transfer (R_{CT}) and diffusion (R_d) contributed to the total polarization resistance (R_p) of the anode, demonstrating that the anode performance are a function of diffusion and kinetic processes. Furthermore, the anodic reaction was much faster than the cathodic at the same current densities based on a comparison of the characteristic frequencies that correspond to the maximum in the imaginary impedance of (Q_{DL}/R_{CT}) between the anode and cathode spectra (Figs. 1B and 2B) [34]. For example, at 7 A m^{-2} the characteristic frequency of the ORR on the cathode was 8 mHz, which was about 43 times smaller than the anodic frequency of 340 mHz. Therefore, while the cathode resistance in 50 mM PBS ($R_{Cat\text{-}50}$ = 17.0 ± 0.1 mΩ m^2) is only slightly larger than that of the anode ($R_{An\text{-}50}$ = 14.6 ± 0.1 mΩ m^2), the bacterial kinetics are surprisingly fast relative to the cathode kinetics. This difference is consistent with an overall view that the sluggish ORR kinetics limits power production in MFCs.

To increase power densities in MFCs treating domestic wastewater, the main challenge is the impact of the low buffer capacity of the wastewater on electrode performance. Although the low ionic conductivity of the wastewater is a challenge, increasing only the conductivity of the solution by adding NaCl did not increase the anode performance [51]. Therefore, adding seawater, for example, to a wastewater at a coastal site would not be expected to improve anode performance. Adding buffer is much more effective, as we showed here that adding phosphate buffer to the SWW substantially increased performance, achieving a 53% decrease in the anode resistance and a 47% increase in the limiting current density. Adding phosphate or even carbonate buffer to a wastewater, however, would not be practical due to environmental impacts of phosphate or the high costs of the buffer. Thus, other methods need to be found to improve electrode performance.

Through identification of the factors limiting the cathode and anode performance by a combined EPS and EIS analysis, it is possible to envision methods by which MFCs treating wastewaters could be improved. AC cathode performance has primarily been enhanced by chemical modifications that increase open cell and working potentials. For example, adding Fe—N—C catalysts to the AC matrix increased the experimental potential from 271 ± 6 mV ($E_{Cat,e0}$) to 442 ± 19 mV, although it did not impact the cathode resistance [9]. This approach therefore gained additional potential from the cathode, but it did not impact the rate of decay in potential with current (i.e. the cathode resistance). While it is unlikely that the ORR kinetics can be improved without increasing the cost or complexity of the electrodes [52], it might be possible to maintain better cathode performance by increasing the electrical conductivity of the AC matrix. For example, adding inexpensive carbon black (CB) to AC cathodes has been shown to improve the maximum power density of MFCs by 36%, (from 1350 ± 50 mW m^{-2} to 1840 ± 20 mW m^{-2}) [53,54]. A key factor in cathode performance will be decreasing the large potential loss at low current densities. Reducing the cathode resistance at low and high current densities may be possible by identifying which sites on the AC matrix are best suited to each RDS, and developing pretreatment methods to maximize the number of sites available for each RDS.

Increasing anode performance could be accomplished through operational changes and anode design. As local pH impacts anode performance, forced flow through the anode should minimize localized pH changes and improve current densities. It has been shown that recirculation through an MFC anode module [55], and even flow forced through the anode of a microbial electrolysis cell (MEC) [56], could improve anode performance. Adding a buffer to a solution would clearly provide a more favorable cathode potential, but buffer addition would not be practical or economical for most wastewaters. High current densities have been achieved in some MFCs where the flow is forced through a thin porous anode [57], although biofilm growth in such configuration could lead to clogging.

Although it was not a focus of this study, a key factor in total power production by MFCs is minimizing energy loss to ohmic resistances. The solution resistance can account for 34% of the internal resistance of MFCs fed with 50 mM PBS and acetate, and 39% for MFCs fed domestic wastewater [9,30]. Reducing the electrode spacing will decrease the solution resistance and the anode will benefit from both decreasing ohmic losses and potentially improved ion exchange between the electrodes, to better maintain pH [58]. However, moving the electrodes closer increases the amount of oxygen reaching the anodic biofilm through the cathode, which can decrease peformance with flat anodes or small diameter brushes [59]. Clearly many factors, including electrode potentials, resistances, and spacing must all be carefully considered in optimizing the peformance of MFCs for long-term stable performance with good power production and efficiency of conversion of organic matter into electrical current.

4. Conclusions

The combined EPS and EIS analysis provided quantifiable and complementary methods to characterize cathode and anode performance. The cathode reaction was shown to be limited by kinetics at high current densities, whereas local pH played an important role at low current densities. Increasing the buffer concentration maintained a circumneutral pH at the cathode, boosting the operative electrode potential. The good agreement between the charge transfer and the polarization resistance of the cathodes revealed that the high internal resistance was only due to the sluggish ORR kinetics on the AC matrix, with no impacts of diffusion of oxygen or hydroxide ions at high current densities. Proton diffusion was a factor in limiting the brush anode performance, increasing the electrode resistance and limiting the maximum current density. Increasing the buffer concentration from 50 mM PBS to 200 mM PBS reduced R_{An} by 64% from 14.6 ± 0.1 mΩ m^2 to 5.3 ± 0.1 mΩ m^2 and increased the limiting current density by 200% from 10.6 ± 0.5 A m^{-2} to 21.5 ± 0.3 A m^{-2}. The diffusion resistance R_d, due to mass-transfer limitations of protons, was limiting the overall anode performance. Wastewater-fed anodes showed lower performance than well buffered acetate-fed anodes, and only increasing buffer concentration enhanced the performance, while there was only a very minimal impact by increasing substrate concentration or solution conductivity.

Notes

The authors declare no competing financial interest.

Acknowledgments

This research was supported by funds provided by the Environmental Security Technology Certification Program, United States via cooperative research agreement W9132T-16-2-0014 through the US Army Engineer Research and Development Center, United States.

B.E.L. and R.R. conceived the idea, R.R. collected the data, R.R, X.W., D.H. and J.M.R. analyzed and interpreted the data and all authors discussed the results and contributed to writing and reviewing the final manuscript.

Appendix A. Supplementary data

Supplementary data to this article can be found online at https://doi.org/10.1016/j.electacta.2020.136330.

Declaration of interests

The authors declare that they have no known competing financial interests or personal relationships that could have appeared to influence the work reported in this paper.

References

[1] A.G. Capodaglio, D. Molognoni, E. Dallago, A. Liberale, R. Cella, P. Longoni, L. Pantaleoni, Microbial fuel cells for direct electrical energy recovery from urban wastewaters, Sci. World J. 2013 (2013), https://doi.org/10.1155/2013/634738.

[2] B.E. Logan, R. Rossi, A. Ragab, P.E. Saikaly, Electroactive microorganisms in bioelectrochemical systems, Nat. Rev. Microbiol. 17 (2019) 307—319, https://doi.org/10.1038/s41579-019-0173-x.

[3] A. Kumar, L.H.H. Hsu, P. Kavanagh, F. Barrière, P.N.L. Lens, L. Lapinsonnière, J.H. Lienhard, U. Schröder, X. Jiang, D. Leech, The ins and outs of

microorganism-electrode electron transfer reactions, Nat. Rev. Chem. 1 (2017) 1–13, https://doi.org/10.1108/10662240210438434.
[4] B.E. Logan, M.J. Wallack, K.Y. Kim, W. He, Y. Feng, P.E. Saikaly, Assessment of microbial fuel cell configurations and power densities, Environ. Sci. Technol. Lett. 2 (2015) 206–214, https://doi.org/10.1021/acs.estlett.5b00180.
[5] W. Yang, K.Y. Kim, P.E. Saikaly, B.E. Logan, The impact of new cathode materials relative to baseline performance of microbial fuel cells all with the same architecture and solution chemistry, Energy Environ. Sci. 10 (2017) 1025–1033, https://doi.org/10.1039/c7ee00910k.
[6] W. Yang, B.E. Logan, Immobilization of a metal – nitrogen – carbon catalyst on activated carbon with enhanced cathode performance in microbial fuel cells, ChemSusChem 9 (2016) 2226–2232, https://doi.org/10.1002/cssc.201600573.
[7] R. Rossi, W. Yang, L. Setti, B.E. Logan, Assessment of a metal–organic framework catalyst in air cathode microbial fuel cells over time with different buffers and solutions, Bioresour. Technol. 233 (2017) 399–405, https://doi.org/10.1016/j.biortech.2017.02.105.
[8] X. Dominguez-Benetton, S. Sevda, K. Vanbroekhoven, D. Pant, The accurate use of impedance analysis for the study of microbial electrochemical systems, Chem. Soc. Rev. 41 (2012) 7228–7246, https://doi.org/10.1039/c2cs35026b.
[9] R. Rossi, B.P. Cario, C. Santoro, W. Yang, P.E. Saikaly, B.E. Logan, Evaluation of electrode and solution area-based resistances enables quantitative comparisons of factors impacting microbial fuel cell performance, Environ. Sci. Technol. 53 (2019) 3977–3986, https://doi.org/10.1021/acs.est.8b06004.
[10] A.J. Hutchinson, J.C. Tokash, B.E. Logan, Analysis of carbon fiber brush loading in anodes on startup and performance of microbial fuel cells, J. Power Sources 196 (2011) 9213–9219, https://doi.org/10.1016/j.jpowsour.2011.07.040.
[11] W. Yang, Y. Peng, Y. Zhang, J.E. Lu, J. Li, S. Chen, Air cathode catalysts of microbial fuel cell by nitrogen-doped carbon aerogels, ACS Sustain. Chem. Eng. 7 (2019) 3917–3924, https://doi.org/10.1021/acssuschemeng.8b05000.
[12] W. Liu, S. Cheng, L. Yin, Y. Sun, L. Yu, Influence of soluble microbial products on the long-term stability of air cathodes in microbial fuel cells, Electrochim. Acta 261 (2018) 557–564, https://doi.org/10.1016/j.electacta.2017.12.154.
[13] G. Yue, K. Meng, Q. Liu, One-step synthesis of N-doped carbon and its application as a cost-efficient catalyst for the oxygen reduction reaction in microbial fuel cells, Chempluschem 80 (2015) 1133–1138, https://doi.org/10.1002/cplu.201500057.
[14] S. Cheng, W. Liu, J. Guo, D. Sun, B. Pan, Y. Ye, W. Ding, H. Huang, F. Li, Effects of hydraulic pressure on the performance of single chamber air-cathode microbial fuel cells, Biosens. Bioelectron. 56 (2014) 264–270, https://doi.org/10.1016/j.bios.2014.01.036.
[15] A. ter Heijne, H.V.M. Hamelers, M. Saakes, C.J.N. Buisman, Performance of non-porous graphite and titanium-based anodes in microbial fuel cells, Electrochim. Acta 53 (2008) 5697–5703, https://doi.org/10.1016/j.electacta.2008.03.032.
[16] X. Zhu, J.C. Tokash, Y. Hong, B.E. Logan, Controlling the occurrence of power overshoot by adapting microbial fuel cells to high anode potentials, Bioelectrochemistry 90 (2013) 30–35, https://doi.org/10.1016/j.bioelechem.2012.10.004.
[17] R. Rousseau, M. Rimboud, M.L. Délia, A. Bergel, R. Basséguy, Electrochemical characterization of microbial bioanodes formed on a collector/electrode system in a highly saline electrolyte, Bioelectrochemistry 106 (2015) 97–104, https://doi.org/10.1016/j.bioelechem.2015.06.011.
[18] C.I. Torres, A.K. Marcus, B.E. Rittmann, Proton transport inside the biofilm limits electrical current generation by anode-respiring bacteria, Biotechnol. Bioeng. 100 (2008) 872–881, https://doi.org/10.1002/bit.21821.
[19] A.E. Franks, K.P. Nevin, H. Jia, M. Izallalen, T.L. Woodard, D.R. Lovley, Novel strategy for three-dimensional real-time imaging of microbial fuel cell communities: monitoring the inhibitory effects of proton accumulation within the anode biofilm, Energy Environ. Sci. 2 (2009) 113–119, https://doi.org/10.1039/b816445b.
[20] A. ter Heijne, O. Schaetzle, S. Gimenez, L. Navarro, B. Hamelers, F. Fabregat-Santiago, Analysis of bio-anode performance through electrochemical impedance spectroscopy, Bioelectrochemistry 106 (2015) 64–72, https://doi.org/10.1016/j.bioelechem.2015.04.002.
[21] Y. Feng, Q. Yang, X. Wang, B.E. Logan, Treatment of carbon fiber brush anodes for improving power generation in air-cathode microbial fuel cells, J. Power Sources 195 (2010) 1841–1844, https://doi.org/10.1016/j.jpowsour.2009.10.030.
[22] R.S. Renslow, J.T. Babauta, P.D. Majors, H. Beyenal, Diffusion in biofilms respiring on electrodes, Energy Environ. Sci. 6 (2013) 595–607, https://doi.org/10.1039/c2ee23394k.
[23] D.R. Bond, S.M. Strycharz-Glaven, L.M. Tender, C.I. Torres, On electron transport through geobacter biofilms, ChemSusChem 5 (2012) 1099–1105, https://doi.org/10.1002/cssc.201100748.
[24] B. Logan, S. Cheng, V. Watson, G. Estadt, Graphite fiber brush anodes for increased power production in air-cathode microbial fuel cells, Environ. Sci. Technol. 41 (2007) 3341–3346, https://doi.org/10.1021/es062644y.
[25] J.L. Stager, X. Zhang, B.E. Logan, Addition of acetate improves stability of power generation using microbial fuel cells treating domestic wastewater, Bioelectrochemistry 118 (2017) 154–160, https://doi.org/10.1016/j.bioelechem.2017.08.002.
[26] S. Cheng, D. Xing, D.F. Call, B.E. Logan, Direct biological conversion of electrical current into methane by electromethanogenesis, Environ. Sci. Technol. 43 (2009) 3953–3958, https://doi.org/10.1021/es803531g.
[27] R. Rossi, W. Yang, E. Zikmund, D. Pant, B.E. Logan, In situ biofilm removal from air cathodes in microbial fuel cells treating domestic wastewater, Bioresour. Technol. 265 (2018) 200–206, https://doi.org/10.1016/j.biortech.2018.06.008.
[28] V.J. Watson, B.E. Logan, Analysis of polarization methods for elimination of power overshoot in microbial fuel cells, Electrochem, Commun. Now. 13 (2011) 54–56, https://doi.org/10.1016/j.elecom.2010.11.011.
[29] F. Zhang, J. Liu, I. Ivanov, M.C. Hatzell, W. Yang, Y. Ahn, B.E. Logan, Reference and counter electrode positions affect electrochemical characterization of bioanodes in different bioelectrochemical systems, Biotechnol. Bioeng. 111 (2014) 1931–1939, https://doi.org/10.1002/bit.25253.
[30] B.E. Logan, E. Zikmund, W. Yang, R. Rossi, K.-Y. Kim, P.E. Saikaly, F. Zhang, Impact of ohmic resistance on measured electrode potentials and maximum power production in microbial fuel cells, Environ. Sci. Technol. 52 (2018) 8977–8985, https://doi.org/10.1021/acs.est.8b02055.
[31] B.P. Cario, R. Rossi, K.Y. Kim, B.E. Logan, Applying the electrode potential slope method as a tool to quantitatively evaluate the performance of individual microbial electrolysis cell components, Bioresour. Technol. 287 (2019) 121418, https://doi.org/10.1016/j.biortech.2019.121418.
[32] J.E. Dykstra, P.M. Biesheuvel, H. Bruning, A. Ter Heijne, Theory of ion transport with fast acid-base equilibrations in bioelectrochemical systems, Phys. Rev. E - Stat. Nonlinear Soft Matter Phys. 90 (2014) 1–10, https://doi.org/10.1103/PhysRevE.90.013302.
[33] F. Alcaide, E. Brillas, P.L. Cabot, EIS analysis of hydroperoxide ion generation in an uncatalyzed oxygen-diffusion cathode, J. Electroanal. Chem. 547 (2003) 61–73, https://doi.org/10.1016/S0022-0728(03)00190-6.
[34] A. Lasia, Electrochemical Impedance Spectroscopy and its Applications, Springer, New York Heidelberg Dordrecht London, 2014, https://doi.org/10.1007/978-1-4614-8933-7.
[35] J. Bisquert, G. Garcia-Belmonte, F. Fabregat-Santiago, P.R. Bueno, Theoretical models for AC impedance of finite diffusion layers exhibiting low frequency dispersion, J. Electroanal. Chem. 475 (1999) 152–163, https://doi.org/10.1016/S0022-0728(99)00346-0.
[36] T.Q. Nguyen, C. Breitkopf, Determination of diffusion coefficients using impedance spectroscopy data, J. Electrochem. Soc. 165 (2018) E826–E831, https://doi.org/10.1149/2.1151814jes.
[37] H. Arai, S. Müller, O. Haas, AC Impedance analysis of bifunctional air electrodes for metal-air batteries, J. Electrochem. Soc. 147 (2002) 3584, https://doi.org/10.1149/1.1393943.
[38] D.B. Zhou, H. Vander Poorten, Electrochemical characterisation of oxygen reduction on teflon-bonded gas diffusion electrodes, Electrochim. Acta 40 (1995) 1819–1826, https://doi.org/10.1016/0013-4686(95)00109-R.
[39] B. Hirschorn, M.E. Orazem, B. Tribollet, V. Vivier, I. Frateur, M. Musiani, Determination of effective capacitance and film thickness from constant-phase-element parameters, Electrochim. Acta 55 (2010) 6218–6227, https://doi.org/10.1016/j.electacta.2009.10.065.
[40] G.J. Brug, A.L.G. van den Eeden, M. Sluyters-Rehbach, J.H. Sluyters, The analysis of electrode impedances complicated by the presence of a constant phase element, J. Electroanal. Chem. 176 (1984) 275–295, https://doi.org/10.1016/S0022-0728(84)80324-1.
[41] E.H. Yu, S. Cheng, B.E. Logan, K. Scott, Electrochemical reduction of oxygen with iron phthalocyanine in neutral media, J. Appl. Electrochem. 39 (2009) 705–711, https://doi.org/10.1007/s10800-008-9712-2.
[42] S.C. Popat, D. Ki, B.E. Rittmann, C.I. Torres, Importance of OH– transport from cathodes in microbial fuel cells, ChemSusChem 5 (2012) 1071–1079, https://doi.org/10.1002/cssc.201100777.
[43] S. Ahn, B.J. Tatarchuk, Air electrode: identification of intraelectrode rate phenomena via AC impedance, J. Electrochem. Soc. 142 (2006) 4169, https://doi.org/10.1149/1.2048480.
[44] D. Malevich, E. Halliop, B.A. Peppley, J.G. Pharoah, K. Karan, Investigation of charge-transfer and mass-transport resistances in PEMFCs with microporous layer using Electrochemical Impedance Spectroscopy, J. Electrochem. Soc. 156 (2008) B216, https://doi.org/10.1149/1.3033408.
[45] E.G. Gagnon, The triangular voltage sweep method for determining double-layer capacity of porous electrodes, J. Electrochem. Soc. 120 (2007) 251, https://doi.org/10.1149/1.2403429.
[46] J.P. Randin, E. Yeager, Differential capacitance study on the basal plane of stress-annealed pyrolytic graphite, J. Electroanal. Chem. 36 (1972) 257–276, https://doi.org/10.1016/S0022-0728(72)80249-3.
[47] R. Karthikeyan, A. Selvam, K.Y. Cheng, J.W.C. Wong, Influence of ionic conductivity in bioelectricity production from saline domestic sewage sludge in microbial fuel cells, Bioresour. Technol. 200 (2016) 845–852, https://doi.org/10.1016/j.biortech.2015.10.101.
[48] S. Georg, I. de Eguren Cordoba, T. Sleutels, P. Kuntke, A. ter Heijne, C.J.N. Buisman, Competition of electrogens with methanogens for hydrogen in bioanodes, Water Res. 170 (2019) 115292, https://doi.org/10.1016/j.watres.2019.115292.
[49] J.Y. Nam, H.W. Kim, K.H. Lim, H.S. Shin, Effects of organic loading rates on the continuous electricity generation from fermented wastewater using a single-chamber microbial fuel cell, Bioresour. Technol. 101 (2010) S33–S37, https://doi.org/10.1016/j.biortech.2009.03.062.
[50] H.S. Lee, P. Parameswaran, A. Kato-Marcus, C.I. Torres, B.E. Rittmann, Evaluation of energy-conversion efficiencies in microbial fuel cells (MFCs) utilizing fermentable and non-fermentable substrates, Water Res. 42 (2008) 1501–1510, https://doi.org/10.1016/j.watres.2007.10.036.
[51] X. Wang, D. Li, X. Mao, E.H. Yu, K. Scott, E. Zhang, D. Wang, Anion exchange

polymer coated graphite granule electrodes for improving the performance of anodes in unbuffered microbial fuel cells, J. Power Sources 330 (2016) 211–218, https://doi.org/10.1016/j.jpowsour.2016.09.019.
[52] E.M. Milner, D. Popescu, T. Curtis, I.M. Head, K. Scott, E.H. Yu, Microbial fuel cells with highly active aerobic biocathodes, J. Power Sources 324 (2016) 8–16, https://doi.org/10.1016/j.jpowsour.2016.05.055.
[53] B. Wei, J.C. Tokash, G. Chen, M.A. Hickner, B.E. Logan, Development and evaluation of carbon and binder loading in low-cost activated carbon cathodes for air-cathode microbial fuel cells, RSC Adv. 2 (2012) 12751–12758, https://doi.org/10.1039/c2ra21572a.
[54] X. Zhang, Q. Wang, X. Xia, W. He, X. Huang, B.E. Logan, Addition of conductive particles to improve the performance of activated carbon air-cathodes in microbial fuel cells, Environ. Sci. Water Res. Technol. 3 (2017) 806–810, https://doi.org/10.1039/c7ew00108h.
[55] R. Rossi, P.J. Evans, B.E. Logan, Impact of flow recirculation and anode dimensions on performance of a large scale microbial fuel cell, J. Power Sources 412 (2019) 294–300, https://doi.org/10.1016/j.jpowsour.2018.11.054.
[56] T.H.J.A. Sleutels, R. Lodder, H.V.M. Hamelers, C.J.N. Buisman, Improved performance of porous bio-anodes in microbial electrolysis cells by enhancing mass and charge transport, Int. J. Hydrogen Energy 34 (2009) 9655–9661, https://doi.org/10.1016/j.ijhydene.2009.09.089.
[57] T.H.J.A. Sleutels, H.V.M. Hamelers, C.J.N. Buisman, Effect of mass and charge transport speed and direction in porous anodes on microbial electrolysis cell performance, Bioresour. Technol. 102 (2011) 399–403, https://doi.org/10.1016/j.biortech.2010.06.018.
[58] S.C. Popat, C.I. Torres, Critical transport rates that limit the performance of microbial electrochemistry technologies, Bioresour. Technol. 215 (2016) 265–273, https://doi.org/10.1016/j.biortech.2016.04.136.
[59] S. Wu, W. He, W. Yang, Y. Ye, X. Huang, B.E. Logan, Combined carbon mesh and small graphite fiber brush anodes to enhance and stabilize power generation in microbial fuel cells treating domestic wastewater, J. Power Sources 356 (2017) 348–355, https://doi.org/10.1016/j.jpowsour.2017.01.041.